



# Through-the-Wall Human Respiration Detection Using UWB Impulse Radar on Hovering Drone

Budiman P. A. Rohman , *Student Member, IEEE*, Muhammad Bagus Andra , *Student Member, IEEE*, and Masahiko Nishimoto, *Member, IEEE*

**Abstract**—The detection of a human being behind obstacles using radar technology has many promising applications, such as postdisaster search and rescue missions. In the case of large observation areas, the use of an unmanned aerial vehicle as the moving platform for radar is an appealing approach. However, this task is challenging because human vital signs provide a relatively weak signal compared with background noise and clutter. The drone's instability also negatively affects the obtained radar signal. Thus, this article presents a new signal processing method to extract and enhance respiration signals from drone-mounted radar. The method works by extracting the analytic signal representation and applying the subspace component segregation. Laboratory experiments in a controlled environment show that the proposed method can suppress a considerable level of vibration generated by unbalanced motor motion and enhance the respiration signal from radar data. A field experimental study using an octocopter in hovering mode confirms the method performs well in real-world conditions.

**Index Terms**—Drone, respiration detection, through-the-wall radar, ultra-wideband (UWB) impulse radar, unmanned aerial vehicle, vital sign detection.

## I. INTRODUCTION

NATURAL disasters occur frequently and can result in both material and nonmaterial losses [1], [2]. In catastrophic cases, large areas are affected with a huge number of victims. Postdisaster search and rescue (SAR) missions play a vital role in evacuating many live survivors quickly, thereby reducing the potential death toll. Advanced technology is necessary to support this mission [3], [4].

Notably, the use of unmanned aerial vehicles or drones for SAR missions in postdisaster environments is of interest to many researchers. This type of technology supports flexibility, mobility, and efficiency in various environments. The modularity

Manuscript received November 1, 2020; revised May 6, 2021; accepted May 26, 2021. Date of publication June 8, 2021; date of current version July 14, 2021. This work was supported by the DRONESAR Project IEEE Geosciences and Remote Sensing Society under IEEE GRSS GSC 2018 program. (*Corresponding author: Budiman P. A. Rohman.*)

Budiman P. A. Rohman is with the Graduate School of Science and Technology, Kumamoto University, Kumamoto 860-8555, Japan, on leave from the Research Center for Electronics and Telecommunication, Indonesian Institute of Sciences, Bandung 40135, Indonesia (e-mail: budi028@lipi.go.id).

Muhammad Bagus Andra is with the Graduate School of Science and Technology, Kumamoto University, Kumamoto 860-8555, Japan (e-mail: andra@ieee.org).

Masahiko Nishimoto is with the Faculty of Advanced Science and Technology, Kumamoto University, Kumamoto 860-8555, Japan (e-mail: nisimoto@cs.kumamoto-u.ac.jp).

Digital Object Identifier 10.1109/JSTARS.2021.3087668



Fig. 1. Developed multisensory drone for disaster SAR mission [7], [8].

of drones means they can carry many different types of sensors, making these unmanned vehicles promising for various specific missions. Researchers have considered employing a radar, lidar, and microphone array into the drone for such purposes instead of the more common camera. The use of such sensors has been shown to offer high performance in both laboratory and field applications [5], [6].

With this potential in mind, we are building a multisensory drone system for supporting SAR missions in complex and chaotic disaster-affected areas [7], [8] (see Fig. 1). This drone is interconnected with a ground control station and a centralized main server. Sensing devices include a microphone array, wide-view camera, and ultra-wideband (UWB) impulse radar. Seeing the feasibility of an on-body tag of radio frequency identification (RFID) technology in the future, we also apply this sensor on the drone. The main purpose of all these sensors is to anticipate any possibility of position and condition of survivors, including visible, audible, buried under destroyed buildings, and pretagged by RFID.

To detect a buried survivor, we adopt through-the-wall detection using a UWB radar technique. This technology is of interest to researchers worldwide due to its many promising applications to fields including law enforcement, military, and SAR missions. However, the development of this technique for actual application in the field faces many problems. The most challenging issue is that human vital signs are weak compared with background noise and surrounding clutter.

Several signal processing techniques have been proposed to account for this problem. In [9] and [10], Xu *et al.* proposed a signal processing technique to improving the level of signal to noise and clutter ratio of the vital signs of a trapped victim. Their method allows the automatic extraction of vital signs. The

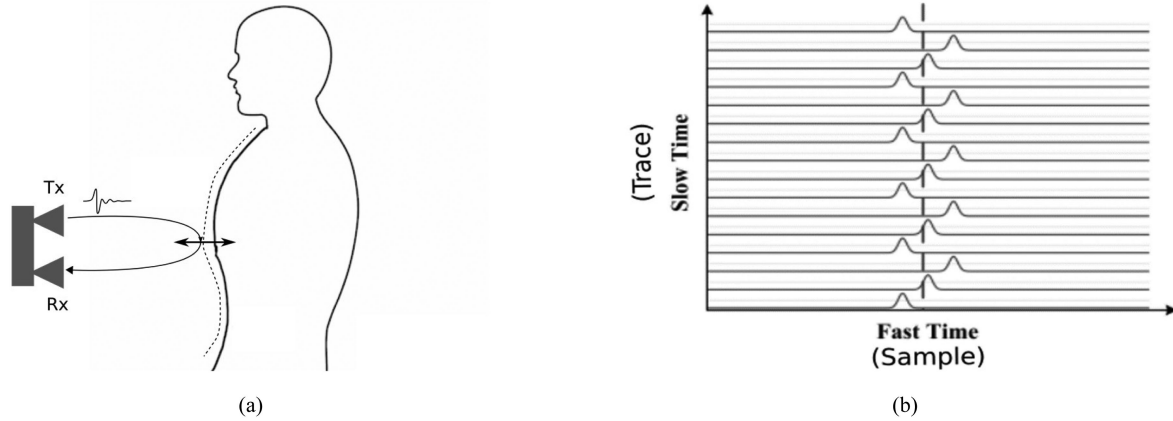


Fig. 2. Vital sign detection using radar. (a) Measurement setup. (b) Recorded radar echo data.

use of subspace decomposition to the recorded radar signal on the time and frequency domain has been proposed in [11] and [12], respectively. This method aims to suppress the clutter by experimentally selecting the appropriate subspace components based on its singular values so that the signals from a human behind a wall can be enhanced. Li *et al.* developed a technique that applies curvelet transform and singular value decomposition (SVD) to enhance and extract human vital signs. Their technique combines Fourier transform, radial Gaussian kernel, Hilbert–Huang transform, and ensemble empirical mode decomposition (EEMD) to extract human respiration and heartbeat from noise in complex environments [13]. Liang *et al.* [14] proposed a complex signal demodulation and frequency accumulation (FA) method to be applied for through-wall vital sign detection and Liang *et al.* proposed an EEMD-based FA technique to determine buried respiration frequency [15].

However, the techniques mentioned above were mostly proposed for static platforms and require data with relatively long duration signals. Certainly, these methods are not intended for drone applications. Furthermore, the possibility that a drone in hovering mode may be unstable, subject to wind, unbalanced bodyweight, deficient compensation control, or rotor-to-rotor interaction [16]–[19] should be considered carefully. Such movement will negatively affect detection performance. Hence, a robust and efficient radar signal processing technique is needed to develop an effective drone SAR system.

To that end, this article proposes a signal processing method for the drone-mounted radar on hovering mode for survivor detection in a postdisaster setting. This study addresses the drone-mounted radar system that is limited by its platform instability. The proposed signal processing modifies the primary signal processing technique used for vital sign detection research as in [9]. Our contribution in this study is developing a new method by applying the analytic representation of the recorded radar signal and singular values clustering by a certain technique and assumption aiming at automatic subspace component segregation on time-domain radar signal. The method has been comprehensively evaluated and tested by laboratory simulation and real-world field studies. To support real-world feasibility and mission efficiency, we consider very short data recording periods of around 4 s, far shorter than those used in previous studies. The

effect of variation of the human respiration speed and strength was also investigated. This study will open a new room for discussing future disaster SAR missions using drone-mounted radar.

The remainder of this article is organized as follows. The problem formulation and system model are explained briefly in Section II followed by the proposed detection technique in Section III. The experimental setup is described in Section IV. The results of this study are explained in Section V. Finally, Section VI concludes the article.

## II. PROBLEM FORMULATION

For vital sign detection in a static environment, a radar system detects changes in target distance corresponding with the delay time of respiration and heartbeat [see Fig. 2(a)]. Therefore, in the receiver antenna, the range measured by the radar  $x(t)$  is expressed by

$$x(t) = x_0 + r(t) = x_0 + A_r \sin(2\pi f_r t) + A_h \sin(2\pi f_h t) \quad (1)$$

where  $x_0$  is a constant range between the radar source and object;  $A_r$  and  $A_h$  are the respiration and heart rate amplitudes, respectively; and  $f_r$ , and  $f_h$  are the corresponding frequencies. However, when the radar is mounted on an unstable platform such as a hovering drone, the total range measured by radar  $x'(t)$  is also affected by the platform movement  $d(t)$  expressed by

$$\begin{aligned} x'(t) &= x(t) + d(t) = x_0 \\ &+ r(t) + d(t) = x_0 + A_r \sin(2\pi f_r t) \\ &+ A_h \sin(2\pi f_h t) \\ &+ A_d \sin(2\pi f_d t) \end{aligned} \quad (2)$$

where  $A_d$  and  $f_d$  are the amplitude and frequency of platform movement, respectively. The propagation time delay  $\tau_v(t)$  of this distance can be expressed by

$$\begin{aligned} \tau_v(t) &= \frac{2x'(t)}{v} = \tau_0 + \tau_r \sin(2\pi f_r t) + \tau_h \sin(2\pi f_h t) \\ &+ \tau_d \sin(2\pi f_d t) \end{aligned} \quad (3)$$

with  $v = 3 \times 10^8$  m/s (the speed of light),  $\tau_0 = 2x_0/v$ ,  $\tau_r = 2A_r/v$ ,  $\tau_h = 2A_h/v$ , and  $\tau_d = 2A_d/v$ . Then, if only one human exists in the detection environment while all other subjects are stationary, then the radar impulse response  $h(\tau, t)$  is given by

$$h(\tau, t) = a_v \delta(\tau - \tau_v(t)) + \sum_i a_i \delta(\tau - \tau_i) \quad (4)$$

where  $\tau$  is the propagation delay,  $a_i \delta(\tau - \tau_i)$  is the signal from the  $i$ th static target with amplitude  $a_i$  and time delay  $\tau_i$ , and  $a_v \delta(\tau - \tau_v(t))$  is the human vital sign motion signal with amplitude  $a_v$  and propagation delay  $\tau_v$ .

If  $s(t)$  is the transmitted signal, then the received signal  $R(\tau, t)$  is defined as

$$R(\tau, t) = s(t) * h(t, \tau) = a_v s(t - \tau_v(t)) + \sum_i a_i s(t - \tau_i). \quad (5)$$

The discrete signals of all reflected signals can be expressed as a two-dimensional (2-D) matrix  $R[m, n]$  of size  $M \times N$ , defined as

$$R[m, n] = a_v s(m\delta_T - \tau_v(nT_s)) + \sum_i a_i s(m\delta_T - \tau_i) \quad (6)$$

where  $T_s$  is the pulse repetition time,  $m = 0, 1, \dots, M-1$  in fast time and  $n = 1, 2, \dots, N-1$  in slow time [see Fig. 2(b)] and  $\delta_T$  sampling interval time. The fast time domain reflects the object's distance while the slow time domain carries respiration information, including its periodic pattern. As its definition, (6) can be represented as

$$\mathbf{R}[m, n] = \mathbf{v}_s[m, n] + \mathbf{b}[m, n] + \mathbf{d}[m, n] + \mathbf{c}[m] \quad (7)$$

where  $\mathbf{v}_s[m, n]$  is the human respiration,  $\mathbf{b}[m, n]$  is the human heartbeat,  $\mathbf{d}[m, n]$  is the drone vibration clutter, and  $\mathbf{c}[m]$  is the static clutter. In this definition, the drone vibration is considered to produce nonstatic clutter that along with other disturbing signals mask the human vital sign detectability.

In real-world settings, the received signal will be contaminated by many interfering signals; thus, the signal  $R[m, n]$  can be expressed by

$$\mathbf{R}[m, n] = \mathbf{v}_s[m, n] + \mathbf{b}[m, n] + \mathbf{d}[m, n] + \mathbf{c}[m] + \mathbf{q}[m, n] + \mathbf{w}[m, n] \quad (8)$$

where  $\mathbf{q}[m, n]$  is a nonstatic clutter and  $\mathbf{w}[m, n]$  is a contaminating white noise. Because the heartbeat is a very weak signal, we consider the respiration signal only. Thus, the purpose of this proposed technique is to extract and detect  $\mathbf{v}_s[m, n]$ , i.e., the respiration sign of a human.

### III. DETECTION TECHNIQUE

The proposed signal processing procedure can be broadly divided into three subprocesses: data acquisition and preprocessing; subspace component segregation; and filtering and detection (see Fig. 3).

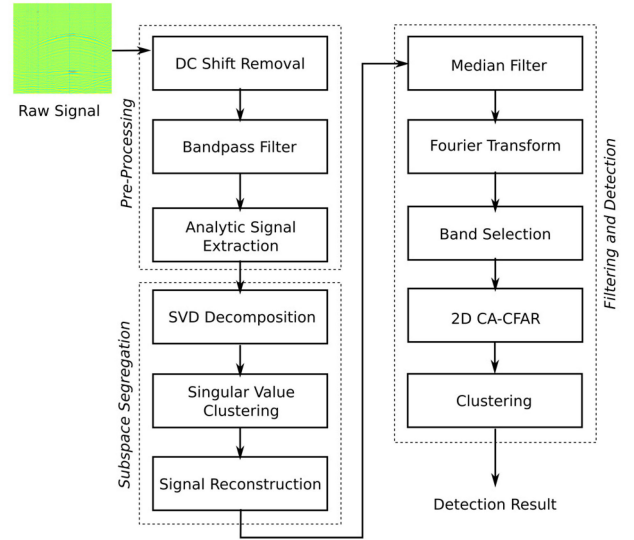


Fig. 3. Proposed signal processing procedure.

#### A. Data Acquisition and Preprocessing

A human vital sign is recorded by radar at a certain duration. After the radar echo recording step, the obtained data is  $\mathbf{R} \in R^{M \times N}$ , a 2-D signal with  $M$  and  $N$  corresponding with the fast and slow time domains, respectively.

As shown in Fig. 3, after the recording step, the signal in the fast time domain is preprocessed using direct current (DC) shift removal. Next, the signal is bandpass filtered using an infinite impulse response filter in a range matching the radar frequency range. Output of these process is  $\hat{\mathbf{R}}$ . In the last step of this subprocessing, we take the analytic signal through a Hilbert transform to obtain the baseband waveform of the preprocessed signal. In this processing, the transformation will reduce signal distortion in the slow time domain. If  $\mathcal{H}$  is Hilbert transform, the analytic signal of signal  $\hat{r}(t)$  can be expressed as

$$\tilde{r}(t) = \hat{r}(t) + i\mathcal{H}\{\hat{r}(t)\} \quad (9)$$

$$\mathcal{H}(\hat{r})(t) = \frac{1}{\pi} P.V. \int_{-\infty}^{+\infty} \frac{\hat{r}(k)}{t-k} dk \quad (10)$$

where P.V. is a Cauchy principal value. The magnitude of the analytic signal will produce the envelope of the radar signal and we take this value for further processing

$$\bar{r}(t) = \|\tilde{r}(t)\|. \quad (11)$$

#### B. Subspace Component Segregation

Because the reflection from walls and other static and/or nonstatic objects will mask the respiration signal, we propose a method to subtract these signals by applying SVD. It is commonly known that by removing the largest singular values from the decomposed radar data, the wall clutter will be suppressed and target signals, including respiration that is contained in the second singular value, can be extracted, easing the further processing steps as in [11] and [12]. Manual and experimental selection is commonly used in this approach. However, the

clutter may extend on the second, third, or other next singular values as concluded in [12] and [13]. Therefore, an accurate selection method of the component is required. The development of this selection method becomes more challenging with the radar mounted on a flying platform system (drone). The instability of the drone and the wide possibility of environmental conditions require an automatic and adaptive singular values selection approach. Thus, we proposed the clustering of singular values for this component selection process. The step of this method is described as follows. As the first step of this process, the 2-D pre-processed radar signal  $\bar{\mathbf{R}}$  is subjected to SVD. This SVD-based method is commonly applied to ground-penetrating radar to remove the ground surface reflection and background noise [22], [23]. This can be written as

$$\bar{\mathbf{R}} = \mathbf{U} \mathbf{S} \mathbf{V} \quad (12)$$

where both  $\mathbf{U} \in R^{M \times M}$  and  $\mathbf{V} \in R^{N \times N}$  are unitary matrices and  $\mathbf{S}$  is a singular matrix consisting of singular values  $(\sigma_1, \sigma_2, \dots, \sigma_r)$ . Equation (12) can be transformed linearly as

$$\bar{\mathbf{R}} = \mathbf{u}_1 \sigma_1 \mathbf{v}_1^T + \mathbf{u}_2 \sigma_2 \mathbf{v}_2^T + \dots + \mathbf{u}_r \sigma_r \mathbf{v}_r^T. \quad (13)$$

In this step, we consider only one-tenth of the ordered decomposed components because the remaining components are very small and not significant.

We assume that the signal obtained contains three main signal components: direct antenna coupling signal  $\mathbf{R}_A$ , wall/barrier reflection signal and clutter  $\mathbf{R}_W$ , and weak signal  $\mathbf{R}_T$

$$\bar{\mathbf{R}} = \mathbf{R}_A + \mathbf{R}_W + \mathbf{R}_T. \quad (14)$$

The weak signal component  $\mathbf{R}_T$  is assumed to contain the respiration signal and very weak contaminating noise. The purpose of this subprocessing is to extract this component.

The first singular value is assumed to correspond to the direct antenna coupling signal

$$\mathbf{R}_A = \mathbf{u}_1 \sigma_1 \mathbf{v}_1^T \quad (15)$$

where  $u_i$ ,  $\sigma_i$ , and  $v_i^T$  are parts of matrix  $\mathbf{U}$ , selected singular values, and parts of matrix  $\mathbf{V}$ , respectively. After removing the first component, the differences of adjacent of remaining squared singular values are then computed as follows:

$$\Delta \sigma_i = \sigma_i^2 - \sigma_{i-1}^2. \quad (16)$$

By this computation, the differences of values became wider and will ease the clustering process. These values are then grouped using a K-means clustering algorithm to create two groups to separate the wall reflection/clutter ( $\mathbf{R}_W$ ) and weak signal ( $\mathbf{R}_T$ ) components. The objective function of this clustering process is Euclidean distance, expressed by

$$J = \sum_{j=1}^{cl} \sum_{i=1}^n \|(\sigma_i)^j - c_j\|^2 \quad (17)$$

where  $J$  is the sum of the error between the clustering centroid and the mean values,  $cl$  the number of clusters,  $c_j$  the centroid of cluster  $j$ , and  $n$  the number of singular values.

Let  $k_1$  be the last index from the remaining components (in descending order) that correspond to  $\mathbf{R}_W$ ; then

$$\mathbf{R}_W = \sum_{i=2}^{k_1} \mathbf{u}_i \sigma_i \mathbf{v}_i^T. \quad (18)$$

The signal components above are then removed from the decomposed signal. Therefore, the remaining component signal  $\mathbf{R}_T$ , containing the respiration and noise signal, can be represented as

$$\mathbf{R}_T = \sum_{i=k_1+1}^r \mathbf{u}_i \sigma_i \mathbf{v}_i^T. \quad (19)$$

Finally, we decompose the obtained radar signal as

$$\bar{\mathbf{R}} = \mathbf{u}_1 \sigma_1 \mathbf{v}_1^T + \sum_{i=2}^{k_1} \mathbf{u}_i \sigma_i \mathbf{v}_i^T + \sum_{i=k_1+1}^r \mathbf{u}_i \sigma_i \mathbf{v}_i^T. \quad (20)$$

### C. Filtering and Detection

In the slow time domain, the signal  $\mathbf{R}_T$  is processed by the median filter to remove the existing noise and normalization producing  $\bar{\mathbf{R}}_T$ . Then, each signal in the slow time domain is converted to the frequency domain by Fast Fourier Transform to detect the human vital sign frequency component

$$\bar{r}_T(\omega) = \int_{-\infty}^{\infty} \bar{r}_T(t) e^{-j\omega t} dt. \quad (21)$$

This calculation at all observed ranges produces  $M \times N$  range-frequency matrix  $\mathcal{R}_T$ .

Because the heartbeat signal is very weak, we only consider the respiration signal in this study. Thus, we establish a window to limit the respiration frequency range. From this spectrum image, we can qualitatively observe the human respiration signal. The next step of the detection technique is to apply the constant false alarm rate (CFAR), a technique commonly used in radar research [24], to establish an adaptive threshold.

We adapt cell-averaging (CA) CFAR as the simplest and most popular method. CA-CFAR works by assuming the binary condition  $H_1$  and  $H_0$  to indicate the presence or absence of the target, respectively

$$H_1 : \mathcal{R}_T[m, n] \geq T \quad (22)$$

$$H_0 : \mathcal{R}_T[m, n] < T. \quad (23)$$

We determine the false alarm rate to compute a threshold, with the average value of several adjacent cells surrounding the cell under test (CUT) used as a reference (see Fig. 4). The CA-CFAR threshold computation can be written as

$$T = \alpha Z, \text{ where } \alpha = N_w (P_{fa}^{-1/N_w} - 1) \quad (24)$$

where  $\alpha$  is a constant value,  $P_{fa}$  is a predetermined value of the probability of false alarm,  $Z$  is the average value of  $N_w$  neighbor cells, and  $N_w$  is the selected number of cells surrounding CUT. The guard cell is also considered in this study to remove the effect of target spectral leakage. The clustering of the signal is then measured to determine the location of the respiration detected.

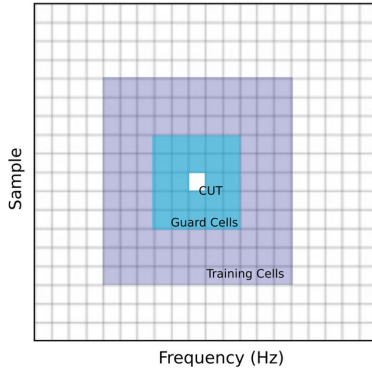


Fig. 4. Two-dimensional CA-CFAR applied in proposed method.

Instead of a comparison of the detection probability, we consider qualitative and quantitative analyses of the spectrum signal. In the quantitative evaluation, we apply the peak factor value determined after the normalization step in the selected region. The peak in this calculation is the respiration frequency. Thus, this is relevant to represent the detectability of a trapped person's respiration. The peak factor  $PF$  is computed as

$$PF = \frac{\|\mathcal{R}_{T_{\max}}\|}{\sqrt{\frac{1}{MN} \sum_{m=1}^M \sum_{n=1}^N |\mathcal{R}_T[m, n]|^2}} \quad (25)$$

where  $\mathcal{R}_{T_{\max}}$  is the peak of the spectrum representing the respiration frequency component,  $\mathcal{R}_T[m, n]$  is the spectrum over the region of detection,  $M$ , and  $N$  is the cell number in the region.

#### IV. EXPERIMENTAL DATA ACQUISITION

We employed Cayenne UWB impulse radar from Novelda [23] for experiments. The transmitted pulse was a monocycle pulse with a bandwidth of 1.5–6 GHz. Each of the datasets consists of around 4 s with a frame rate of around 140 fps. Each trace had 512 sample points with a sample rate of around 39E9 samples per second. In the free space, the maximum distance of each trace was around 2 m with a resolution of 4 mm.

The barrier for our laboratory simulation was a layer of wood block, clay brick, and cement brick wall (see Fig. 5). We used an artificial respiration actuator imitating human chest displacement during respiration. The displacement  $d_r$  was 3, 6, and 10 mm with a frequency  $f_r$  of 0.3, 0.6, and 0.8 Hz. These parameters follow actual respiration phenomena [26], [27]. We used a paper sheet to simulate human skin.

To simulate drone vibration in the laboratory experiment, we applied unbalanced motors on the right and left sides of the radar mount. By tuning the voltage feed to the motor, the rotation speed will change such that the vibration could be varied, changing of frequency and amplitude. We used voltage  $V_f$  in a range of 2.5–5 V. The generated vibration was also recorded by a three-axis accelerometer in the bottom of the unbalanced motor. We used a SensorTile STEVAL-STLKT01V1 accelerometer from ST Microelectronics [28]. The placement of the accelerometer in both the laboratory experimental setup and drone is shown in Fig. 6.

The experiment used a drone that was modified and developed by us as described in [7] and [8]. The basic structure of the drone

before modification is an octocopter with a diameter of around 1 m. The frame is a Tarot X8 TL8X000 equipped with brushless motor XT-Xinte 5010 350 KV, Hobbywing XRotor Pro 40 A as speed controllers, and Tarot TL100D03 as propellers. For the flight/autopilot controller, we used a DJI Naza M V2 equipped with an inertial measurement unit and a global positioning system. This drone can hover in a relatively stable manner; hence, even in a considerably windy environment, it should vibrate smoothly. We worked with the drone outdoors, using the respiration actuator buried under the cement block and wood layer. The signal processing was computed offline after the data recording process to minimize risk as the drone was controlled by an amateur pilot.

#### V. RESULT

Evaluation of the proposed method is described from five perspectives. First, the result of each step of signal processing is investigated. Second, the effect of the platform vibration on the spectrum signal and peak factor is studied. Third, the generality of the method against the variation of the human respiration's strength and speed is investigated. Fourth, we checked the probability of detection value as a quantitative evaluation of method performance. Finally, the applicability of the method is checked by using data collected using real drone-borne radar. We use two existing peer-reviewed methods as a baseline for comparison. The first reference method (Baseline 1) is the basis of this developed method taken from [9]. Then, the Baseline 2 method is the existing method described in [11] that works by removing the largest singular value of a subspace component of decomposed radar signal on the time domain signal aiming to enhance detection of a breathing human.

##### A. Results for Each Signal Processing Step

Fig. 7 shows the results of the proposed signal processing approach. Fig. 7(a) shows the signal after data acquisition and DC removal; the respiration signal is not yet visible. The image with the analytic signal is extracted [see Fig. 7(b)] and the singular value segregation is held after this step, resulting in Fig. 7(c). The vital sign pattern is still not visible. However, median filter and FFT enable us to see the frequency component to distinguish the respiration signal from other signals, with the result shown in Fig. 7(e). From these figures, we can see the dominant frequency of the respiration signal. Then, by applying 2-D CA-CFAR, we can detect exactly and locate the presence of a respiration signal as seen in Fig. 7(f). Comparing with the actual value, the detected center frequency of respiration is shifted to be higher; this is a result of the vibration and processing, including smoothing. The instability of radar sampling time due to vibration may also contribute. However, the shift value is still acceptable for our purposes.

##### B. Effect of Platform Vibration

The drone vibration produces variability of the distance between the radar, wall/barrier, and the human chest, which could produce an artifact that could be confused with human respiration. In the laboratory experiment, we applied simulated

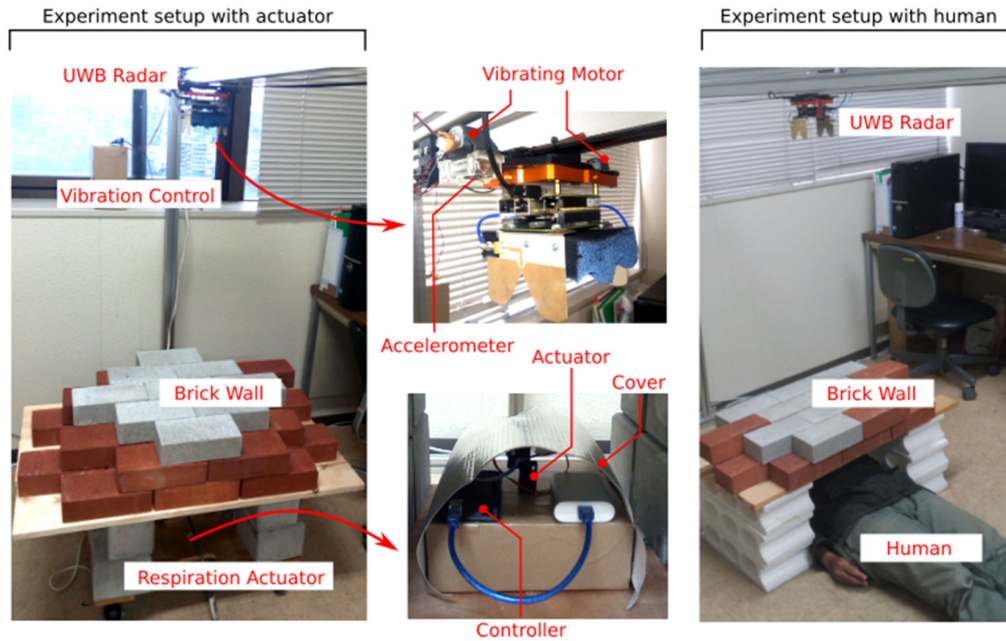


Fig. 5. Experimental setup in the laboratory environment.

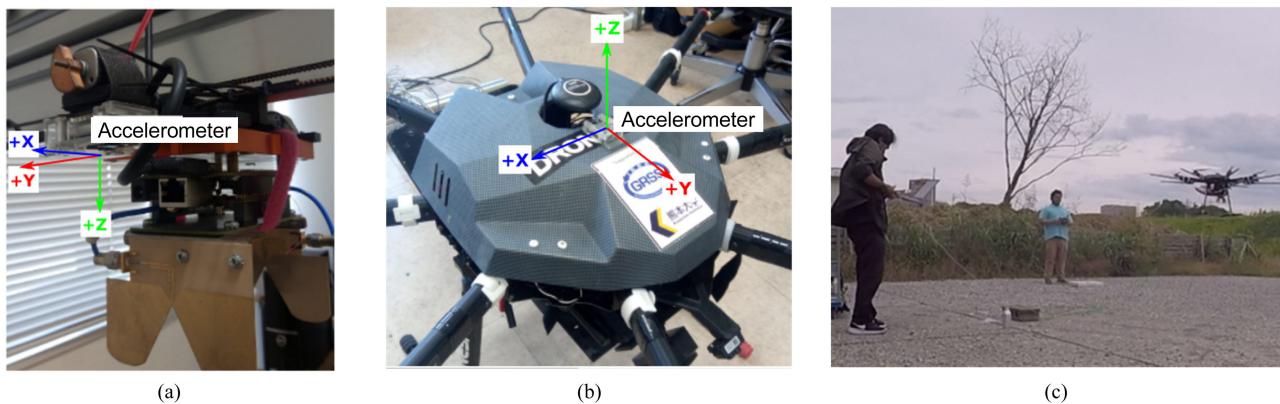


Fig. 6. Vibration measurement using an accelerometer in a: (a) laboratory setup, (b) drone, and (c) setup for drone vibration measurement.

vibration on the radar platform. The response to vibration generated with different voltages was recorded using an accelerometer [see Fig. 8(a)–(h)]. With high-voltage vibration, the vibration amplitude increased. In the frequency domain, some peaks appeared sporadically at several frequencies during lower voltage vibration. The recorded accelerometer data from the hovering drone [see Fig. 8(i) and (j)] show a similar vibration pattern, indicating that the vibration generated in the laboratory experiment is relatively representative of the real hovering drone.

Table I compares the spectrum produced by a real human and that produced by the respiration actuator. This table also compares the result of the proposed method with existing baseline methods. From this table, we can observe that the real human source and actuator display relatively similar patterns. This feature can be seen on all observed methods. Thus, we can confirm that the developed actuator is representative enough to imitate the real human respiration motion.

Table II shows the performance in terms of the produced spectra of the reference and proposed signal processing techniques in detecting the buried respiration using data collected, with vibration simulated with various feed voltages. These results show, as expected, that such vibration can generate nonstationary clutter, thus masking the respiration signal. Moreover, the higher voltage of vibration feed makes the signal noisier and the respiration signals more difficult to detect. However, in the same observed condition, mostly, the proposed method can better suppress the noise and clutter, and thus enhance the respiration signal, than the baseline methods. The comparison of spectral images and peak factor values confirms this result.

Respiration strength and frequency should also affect the detectability of respiration. Table III compares the performance of the baseline and proposed methods. Stronger respiration is less affected by platform vibration. However, when respiration is weak and slow, the vibration of the platform will disturb the

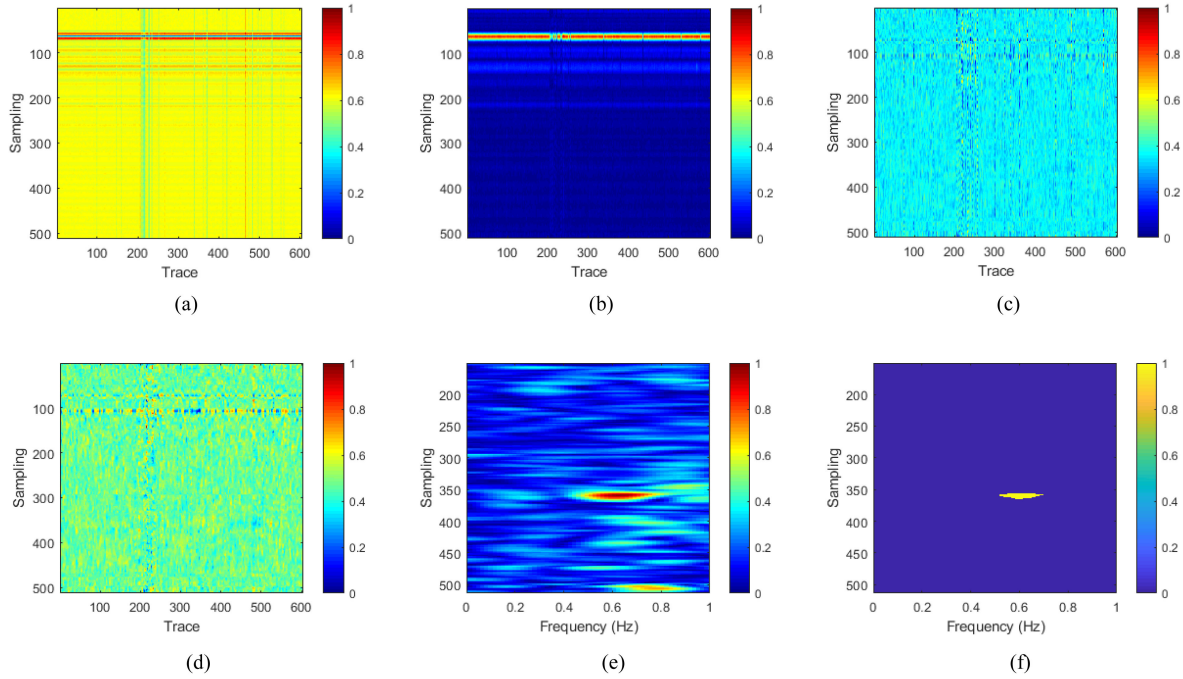


Fig. 7. Result of proposed signal processing step of buried respiration with  $f_r = 0.6$  Hz,  $d_r = 3$  mm,  $V_f = 5$  V. (a) Raw data after dc removal. (b) After preprocessing and analytic signal extraction. (c) After subspace component segregation. (d) After median filtering in the fast time domain. (e) Spectrum signal. (f) After 2D CA-CFAR thresholding with  $P_{fa} = 2E-2$ .

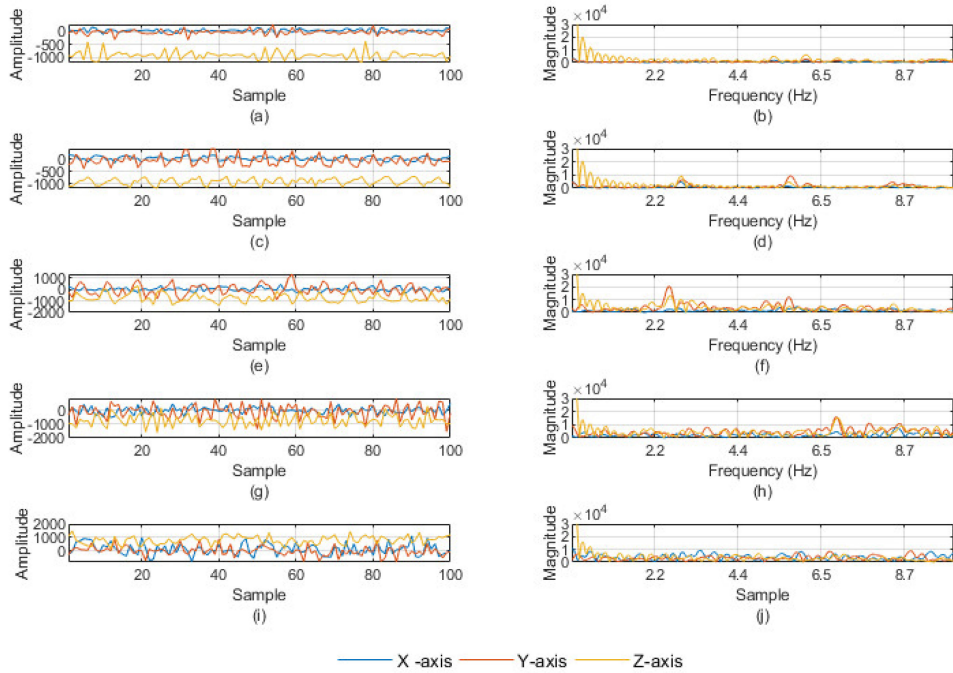


Fig. 8. Vibration data from different power levels recorded by accelerometer; each pair of figures shows the time and frequency domain representations. (a) and (b) 2.5 V. (c) and (d) 3 V. (e) and (f) 4 V. (g) and (h) 5 V. (i) and (j) Hovering drone.

clarity of the signal more significantly. However, the proposed method still can enhance the clarity of the respiration signal even in the most difficult cases such as in the case  $f_r = 0.8$  Hz,  $d_r = 3$  mm (last row). Moreover, this method works better than the reference methods in terms of both spectrum signal and peak factor evaluation.

### C. Effect of Complex Barriers

In a real disaster environment, the wall surfaces may be very chaotic, complex, and composed of many materials. Therefore, to investigate the applicability of the method in such scenarios, we tested our method in imitated conditions in our laboratory

TABLE I  
COMPARISON OF SPECTRAL IMAGES OF RESPIRATION BETWEEN REAL HUMAN AND ACTUATOR

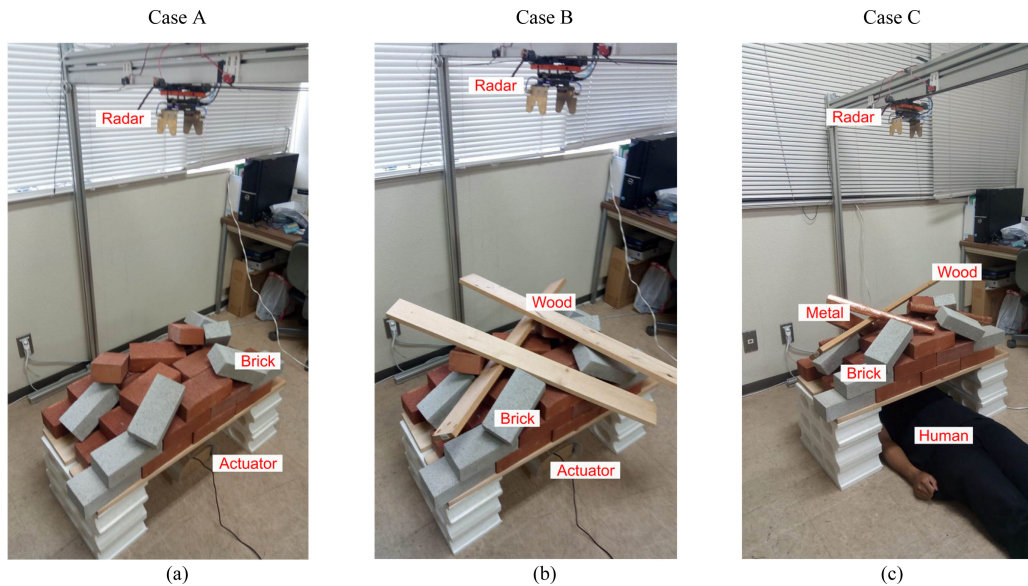
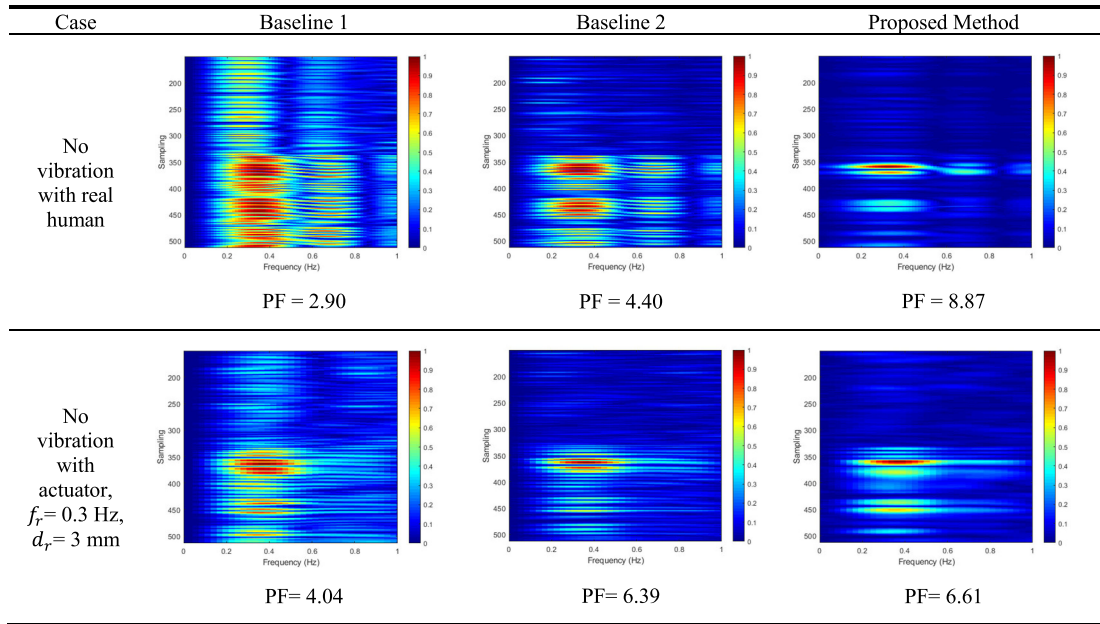


Fig. 9. Experimental setup for evaluating the barrier situations. (a) Chaotic bricks with actuator. (b) Chaotic bricks and woods with actuator. (c) Chaotic bricks, woods, and metallic pipe with real human.

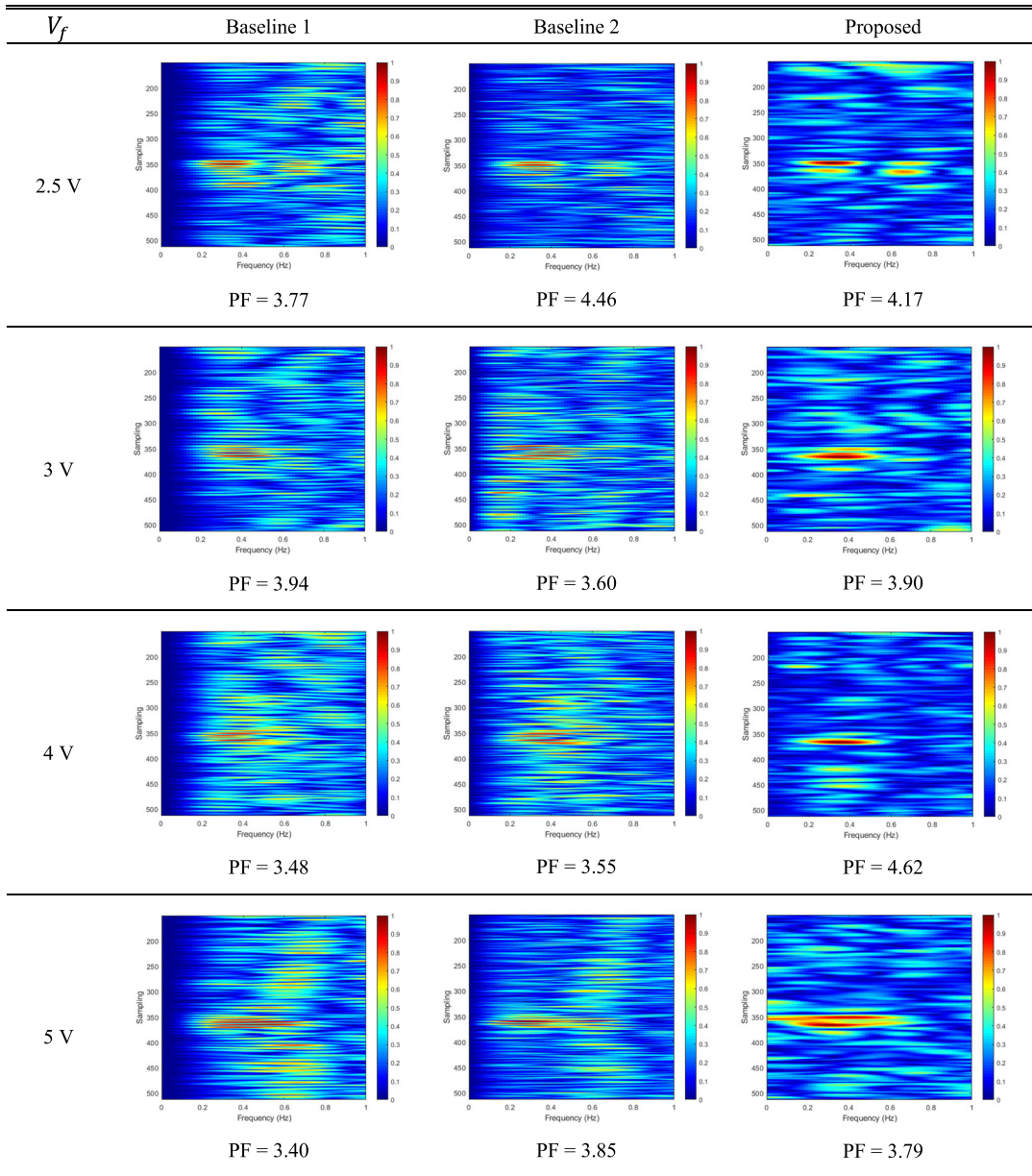
environment. We simulated three random chaotic surface environments with simulated drone vibration using both the respiration actuator and a real human. The respiration actuator uses frequency  $f_r = 0.6$  Hz and displacement  $d_r = 3$  mm, and platform vibration feed voltage  $V_f = 5$  V. The real human respiration frequency is around 0.38 Hz. As a physical barrier, we used random combinations of bricks, wood, and metallic pipes in each case. Photographs of the three setups are shown in Fig. 9. Then, we check the frequency component after the signal processing step shown in Table IV. As seen in Table IV, by using the baseline methods, the respiration frequency

component can be seen but not clearly; many disturbing noises are surrounding the dominant frequency. However, when using the proposed method, the spectrum is clearer, and we can detect the respiration frequency component. It seems that the noises made by both vibration and material reflections were successfully eliminated in our signal processing step. Thus, the proposed method is reliable enough in the face of both platform vibration and a chaotic barrier structure.

We understand that the real situation in the disaster-stricken area may be much more complex and chaotic compared with this simulated condition. However, seeing current experimental



TABLE II  
COMPARISON OF SPECTRAL IMAGES OF RESPIRATION WITH ACTUATOR  $f_r = 0.3$  Hz,  $d_r = 3$  mm ON VIBRATING PLATFORM



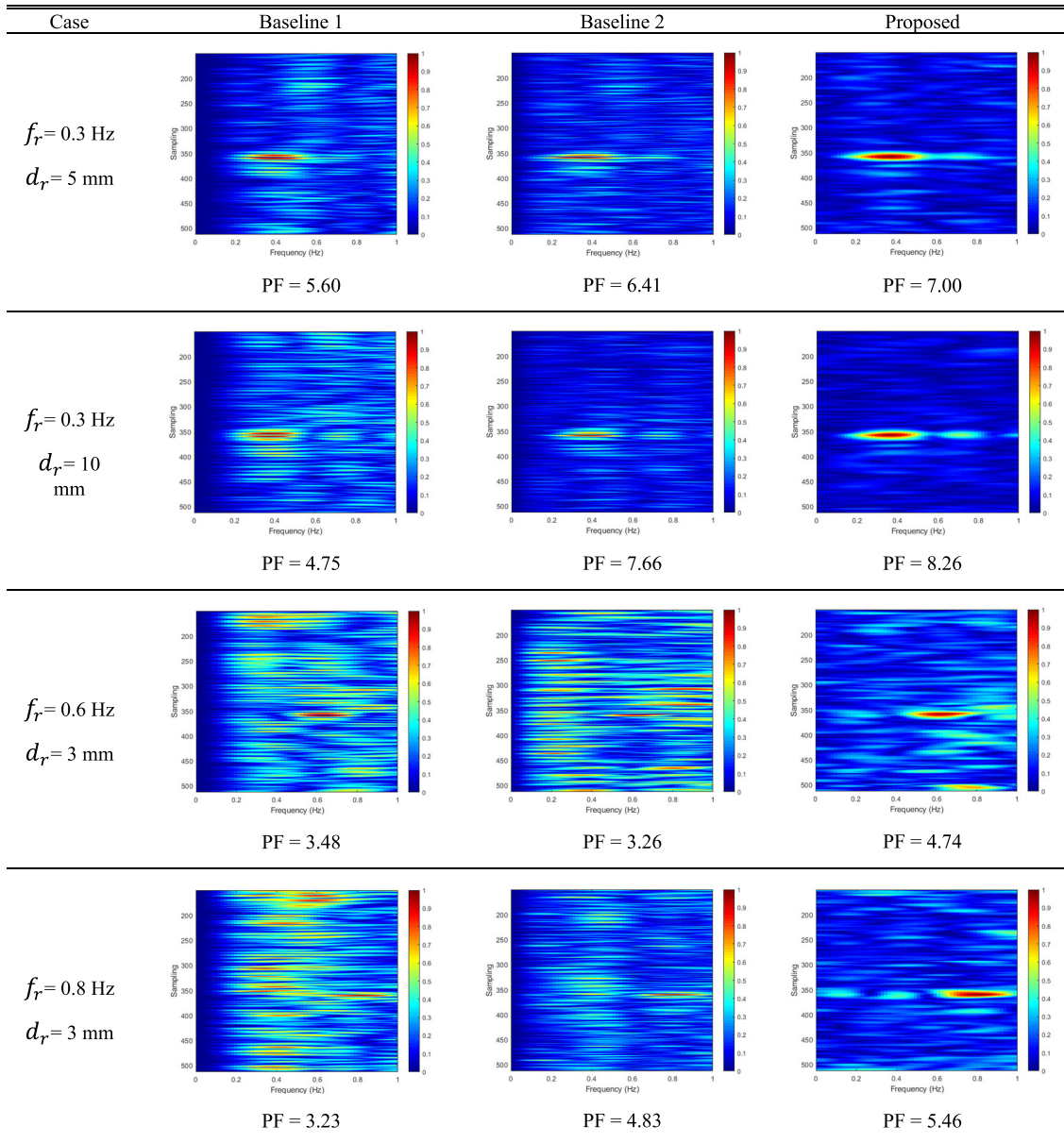
results, we believe that the method will still work with higher performance than the existing baseline methods.

#### D. Comparison of Detectability

In the CA-CFAR threshold step, we must determine the size of training cells, guard cells, and the probability of false alarm. Because there is no established rule for these parameters, we determined it experimentally. According to our numerical experiments, the best configuration for this scheme is training cells:  $x = 10$  cells,  $y = 12$  cells; and guard cells:  $x = 8$  cells,  $y = 8$  cells. The change of probability of false alarm value will be investigated to see its effect on the detection rate. In this test, the actual respiration signal from the actuator was at a frequency of 0.6 Hz with a displacement of 3 mm located in a sample of

around 350 samples in fast time domain. To accommodate any shift in both frequency and range of respiration, in this analysis, we assume respiration has a frequency range of 0.55–0.65 Hz and a sampling range of 340–370 samples. The test is taken on the respiration signal with a vibrating radar platform by feeding a voltage  $V_f$  of 5 V. The frame number in this test is 500 frames, each with a duration of approximately 4 s. In this study, we considered the probability of a false alarm  $P_{fa}$  as  $2E-1$ ,  $2E-2$ , and  $2E-3$ . Of course, a high probability of false alarm will increase the detection rate and vice versa. Hence, in the real application, this value should be determined carefully to obtain an acceptable low false alarm rate with as high as possible detection rate. The comparison of the probability of detection by applying an equal CFAR setup is shown in Table V. In the high false alarm rate ( $2E-1$ ), all the investigated methods

TABLE III  
COMPARISON OF SPECTRAL IMAGES IN DIFFERENT RESPIRATION CONDITIONS WITH VIBRATION AT 5 V



detected the presence of a respiration signal. However, when the false alarm rate was set to be very lower ( $2E-3$ ), the proposed method detectability was superior to the baseline methods. Our method can increase the peak factor of the respiration frequency to the background clutter and noises, improving detectability. This result confirms our previous investigations shown in Tables I–IV.

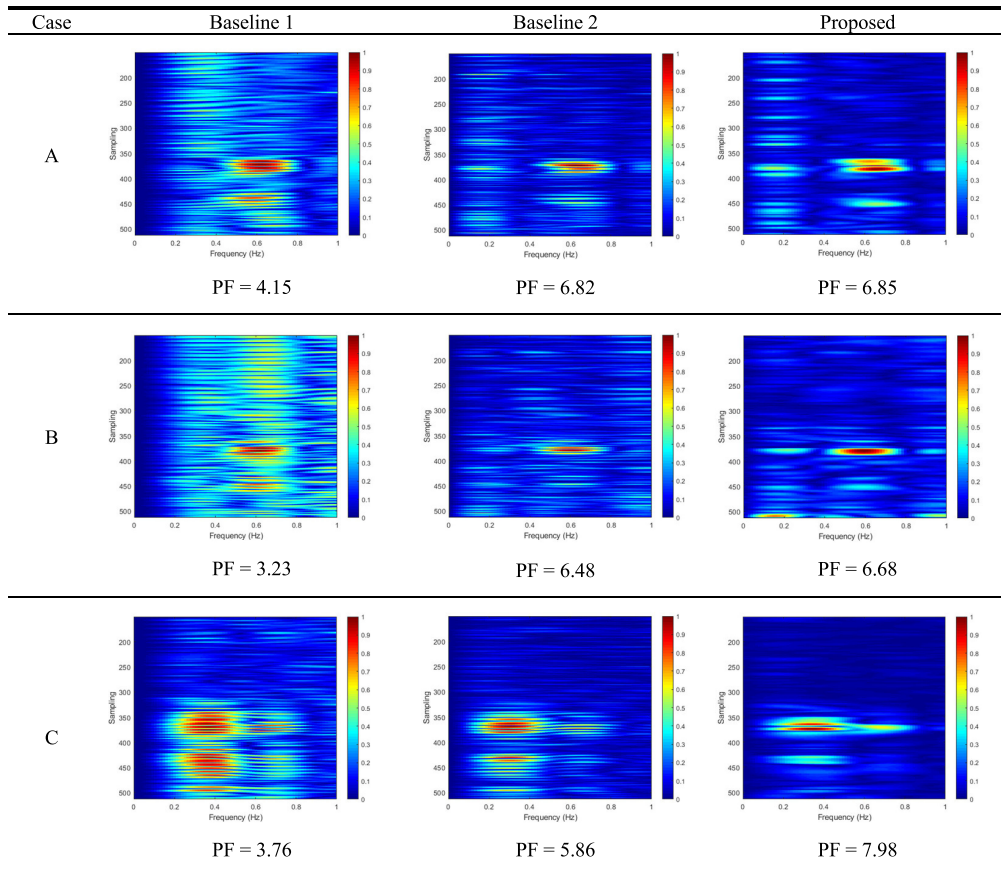
### E. Field Experiments Using the Drone

The frequency component of the drone vibration spreads over the respiration frequency range with almost constant amplitude (see Fig. 8). This affects the detected distance to the object and produces a white noise-like interference with the original signal. This behavior is similar to the vibration generated by our

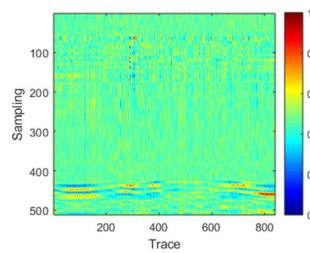
laboratory setup. Thus, intuitively, the result of signal processing should be similar between the simulated and real drone vibration.

To confirm this, we applied our method to real field experiment data. Fig. 10 shows the field experimental setup and the signal processing results. Fig. 10(a) shows the drone hovering at a constant height of around 1.5 m. The results in the time and frequency domain after processing using baseline and proposed methods are shown in Fig. 10(b)–(e). A dominant frequency signal around 0.6 Hz is evident, the same respiration actuator frequency noted under laboratory conditions. The result in Fig. 10(e) indicates that our method is applicable to data collected in real-world conditions using the developed octocopter system [7], [8]. The figure also shows that our method, in this case, can produce a clearer image than the baseline methods.

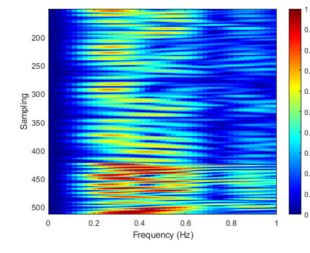
TABLE IV  
COMPARISON OF SPECTRAL IMAGES WITH SIMULATED CHAOTIC BARRIER AND PLATFORM VIBRATION AT 5 V



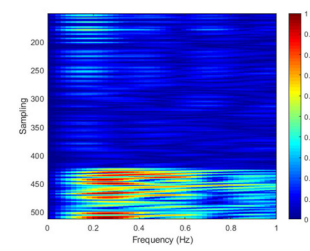
(a)



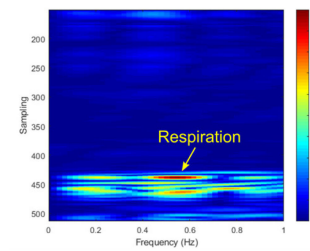
(b)



(c)



(d)



(e)

Fig. 10. Experiment with drone. (a) Experimental setup. (b) Time domain signal. (c)–(e) Spectrum signal from Baseline 1, Baseline 2, and proposed method, respectively.

TABLE V  
COMPARISON OF PROBABILITY OF DETECTION WITH VIBRATION AT 5 V

Method	Probability of Detection (%)		
	$P_{fa} = 2E-1$	$P_{fa} = 2E-2$	$P_{fa} = 2E-3$
Baseline 1	100	74.0	0
Baseline 2	100	100	5.2
Proposed	100	94.8	88.8

## VI. CONCLUSION

This article describes an experimental study seeking to detect buried human respiration using UWB impulse radar mounted on a hovering drone. We proposed a signal processing method that uses analytic signal representation and subspace component segregation by K-means clustering techniques. Considering the limitations of data collected by a hovering drone, this method aimed to use very short duration data collected from an unstable radar platform. The experimental study conducted in the laboratory shows that the proposed method can detect the presence of respiration under obstacles. In the same observed cases, including simulated chaotic barriers, this method provided better performance than the baseline methods. The proposed method also exhibited superiority on a wide range of simulated respiration strengths and frequencies. The signal processing data could also extract buried respiration signals from real field data collected using the developed octocopter. These results confirm the effectiveness and applicability of the proposed method.

However, some limitations in this method should be considered carefully. First, in this study, we considered a relatively stable drone with relatively minor vibration during hovering. A different type or size of drone would provide different performance. Significant vibration will affect the distortion of the echo radar signal and decrease the detectability of respiration signals. We also must note that the experiments took place in a dry environment. Because wet medium will attenuate radar signal power, respiration signals may be more difficult to detect. Therefore, it may be difficult to apply this approach in cases such as finding buried survivors of landslides due to floods or heavy rain. Further study should focus on such situations. This developed method employs subspace decomposition and clustering that consequently will add the complexity and processing time. However, seeing that the method can improve signal clarity and detection performance in a wide possible environment, the computation time can be justified. Moreover, as computer processors became faster and more economical even in a very compact size, the method is feasible to be applied.

We understand that the conditions in a disaster-stricken area in a real situation may be very complex and chaotic, much more complex than the simulated cases. Of course, in such conditions, the accuracy of detection may decrease. Nevertheless, the results of this study indicate that the method should still work even cannot show its best performance. Besides, the method works better than the baseline methods in the same observed case.

In this study, we used a commercial-off-the-shelf radar. It is also possible to apply specialized radar systems for such applications. Customizations, such as changes to frequency range and center frequency, can be applied to maximize depth detection

ability and resolution. The use of software-defined radio-based radar could also be investigated.

## ACKNOWLEDGMENT

The authors would like to thank IEEE IMS, IEEE Sensors Council and ST Microelectronics for providing SensorTile development kit for NPWS project under IEEE IS&M-SC 2018 program that was used for vibration measurement in this work.

## REFERENCES

- [1] Japan quake: Loss and recovery in numbers, BBC News, Mar. 2012. Accessed on: Sep. 26, 2019. [Online]. Available: <http://www.bbc.com/news/world-asia-17219008>
- [2] *Indonesia Earthquakes Kills More Than 100 in Aceh Province*, New York, NY, USA Times, Dec. 2016. Accessed on: Sep. 26, 2019. [Online]. Available: <https://www.nytimes.com/2016/12/07/world/asia/indonesia-earthquake-aceh-sumatra.html>
- [3] Y. Liu and G. Nejat, "Robotic urban search and rescue: A survey from the control perspective," *J. Intell. Robot. Syst.*, vol. 72, no. 2, pp. 147–165, 2013.
- [4] S. Waharte and N. Trigoni, "Supporting search and rescue operations with UAVs," in *Proc. Int. Conf. Emerg. Secur. Technol.*, 2010, pp. 142–147.
- [5] D. R. A. Almeida *et al.*, "Monitoring the structure of forest restoration plantations with a drone-lidar system," *Int. J. Appl. Earth Observ. Geoinf.*, vol. 79, pp. 192–198, 2019.
- [6] M. Wakabayashi, H. G. Okuno, and M. Kumon. "Multiple sound source position estimation by drone audition based on data association between sound source localization and identification." *IEEE Robot. Automat. Lett.*, vol. 5, no. 2, pp. 782–789, Apr. 2020.
- [7] B. P. A. Rohman, M. B. Andra, H. F. Putra, D. H. Fandiantoro, and M. Nishimoto, "Multisensory surveillance drone for survivor detection and geolocalization in complex post-disaster environment," in *Proc. IEEE Int. Geosci. Remote Sens. Symp.*, Jul. 2019, pp. 9368–9371.
- [8] M. B. Andra, B. P. A. Rohman, and T. Usagawa, "Feasibility evaluation for keyword spotting system using mini microphone array on UAV," in *Proc. IEEE Int. Geosci. Remote Sens. Symp.*, Jul. 2019, pp. 2264–2267.
- [9] Y. Xu, S. Wu, C. Chen, J. Chen, and G. Fang, "A novel method for automatic detection of trapped victims by ultrawideband radar," *IEEE Trans. Geosci. Remote Sens.*, vol. 50, no. 8, pp. 3132–3142, Aug. 2012.
- [10] Y. Xu, J. Shao, J. Chen, and G. Fang, "Automatic detection of multiple trapped victims by ultra-wideband radar," *IEEE Geosci. Remote Sens. Lett.*, vol. 10, no. 6, pp. 1498–1502, Nov. 2013.
- [11] S. Singh *et al.*, "Sense through wall human detection using UWB radar," *EURASIP J. Wireless Commun. Netw.*, vol. 20, pp. 1–11, Jun. 2011.
- [12] A. Nezirovic, A. G. Yarovoy, and L. P. Ligthart, "Signal processing for improved detection of trapped victims using UWB radar," *IEEE Trans. Geosci. Remote Sens.*, vol. 48, no. 4, pp. 2005–2014, Apr. 2010.
- [13] F. H. C. Tivive, A. Bouzerdoum, and M. G. Amin, "An SVD-based approach for mitigating wall reflections in through-the-wall radar imaging," in *Proc. IEEE RadarCon*, May 2011, pp. 519–524.
- [14] J. Li, L. Liu, Z. Zeng, and F. Liu, "Advanced signal processing for vital sign extraction with applications in UWB radar detection of trapped victims in complex environments," *IEEE J. Sel. Topics Appl. Earth Observ. Remote Sens.*, vol. 7, no. 3, pp. 783–791, Mar. 2014.
- [15] X. Liang *et al.*, "Ultra-wideband impulse radar through-wall detection of vital signs." *Sci. Rep.*, vol. 8, no. 13367, pp. 1–20, 2018.
- [16] X. Liang *et al.*, "Improved denoising method for through-wall vital sign detection using UWB impulse radar," *Digit. Signal Process.*, vol. 74, pp. 72–93, 2018.
- [17] J. Verbeke and S. Debruyne, "Vibration analysis of a UAV multirotor frame," *Proc. ISMA Int. Conf. Noise Vib. Eng.*, Sep. 2016, pp. 2329–2337.
- [18] C. R. Russell *et al.*, "Wind tunnel and hover performance test results for multicopter UAS vehicles," Accessed on: Sep. 26, 2019. [Online]. Available: <https://ntrs.nasa.gov/citations/20160007399>
- [19] W. H. Semke and M. D. Dunlevy, "A review of the vibration environment onboard small unmanned aircraft," *Sensors Instrum., Aircr./Aerosp. Energy Harvesting*, vol. 8, pp. 155–164, 2019.
- [20] W. Zhou *et al.*, "An experimental investigation on rotor-to-rotor interactions of small UAV propellers," in *Proc. 35th AIAA Appl. Aerodyn. Conf.*, 2017, Paper 2017-3744.

- [21] B. P. A. Rohman and M. Nishimoto, "Ground clutter suppression in GPR using framing based mean removal and subspace decomposition," in *Proc. Int. Symp. Antennas Propag.*, 2017, pp. 1–2.
- [22] C. Liu, C. Song, and Q. Lu, "Random noise de-noising and direct wave eliminating based on SVD method for ground penetrating radar signals," *J. Appl. Geophys.*, vol. 144, pp. 125–133, 2017.
- [23] B. P. A. Rohman and M. Nishimoto, "GPR target signal enhancement using least square fitting background and multiple clustering of singular values," *Prog. Electromagn. Res. Lett.*, vol. 83, pp. 123–132, 2019.
- [24] B. P. A. Rohman and D. Kurniawan, "Neural network-based adaptive selection CFAR for radar target detection in various environments," *Int. J. Intell. Syst. Technol. Appl.*, vol. 18, no. 4, pp. 377–390, 2019.
- [25] *Cayenne Radar Development Kit Bow Tie*. Accessed: Sep. 26, 2019. [Online]. Available: <https://store.flatearthinc.com/products/cayenneradar-development-kit>
- [26] Q. Lindh *et al.*, *Delmar's Comprehensive Medical Assisting: Administrative and Clinical Competencies*. Boston, MA, USA: Cengage Learning, 2013, pp. 573.
- [27] T. Kondo *et al.*, "Laser monitoring of chest wall displacement," *Eur. Respir. J.*, vol. 10, no. 8, pp. 1865–1869, 1997.
- [28] STEVAL-STLKT01V1ST SensorTile development kit. Accessed on: Sep. 26, 2019. [Online]. Available: <https://www.st.com/en/evaluation-tools/steval-stlkt01v1.html#overview>



**Budiman P. A. Rohman** (Student Member, IEEE) received the B.E. degree in engineering physics from Institut Teknologi Sepuluh Nopember, Surabaya, Indonesia, in 2009, and the M.E. degree in computer science and electrical engineering from Kumamoto University, Kumamoto, Japan, in 2018, where he is currently working toward the Ph.D. degree for study on ultra-wideband radar signal processing and imaging.

In 2015, he joined the Research Center for Electronics and Telecommunication, Indonesian Institute of Sciences, Bandung, Indonesia, while currently he is temporarily absent from his work for studying in Kumamoto University. His research interests include signal processing, radar signal processing, radar imaging, machine learning and embedded systems.



**Muhammad Bagus Andra** (Student Member, IEEE) received the B.E. degree from Institut Teknologi Sepuluh Nopember, Surabaya, Indonesia, in 2015, and the M.E. degree in computer science and electrical engineering from Kumamoto University, Kumamoto, Japan, where he is currently working toward the Ph.D. degree in computer science.

He is a member of Human Interface Cyber Communication Laboratory. His research interests include signal processing, speech processing, natural language processing, and machine learning.

Mr. Andra is a member of Acoustical Society of Japan.



**Masahiko Nishimoto** (Member, IEEE) received the B.E. degree in electronic engineering from Kumamoto University, Kumamoto, Japan, in 1982, and the M.E. and D.E. degrees in computer science and communication engineering from Kyushu University, Fukuoka, Japan, in 1984 and 1987, respectively.

Since 1987, he has been with the Department of Electrical Engineering and Computer Science, Kumamoto University, and he is currently a Professor with Faculty of Advanced Science and Technology, Kumamoto University. From 2001 to 2002, he was a Visiting Scholar with Duke University, Durham, NC, USA. From 2009 to 2010, he served as an IEEE AP-S Fukuoka Chapter Chair, and from 2011 to 2013, he served as the Chair of the Technical Committee on Electromagnetic Theory in Electronics Society of the IEICE. His research interests include the area of radar signal processing, application of ground penetrating radar, scattering and diffraction of electromagnetic waves, and computational electromagnetics.